Electronic Supplementary Material (ESI) for Nanoscale.

Supporting Information

High-sorption terpyridine-graphene oxide hybrids for efficient removal of heavy metal ions from wastewater

Dawid Pakulski, Adam Gorczyński, Dawid Marcinkowski, Włodzimierz Czepa, Tomasz Chudziak, Samanta Witomska, Yuta Nishina, Violetta Patroniak, Artur Ciesielski, and Paolo Samorì

Table of Content **Page**

Tables

Adsorbent	**Contaminant**	**Maximum capacity [mg g^{-1}]**	**Temperature [K]**	**pH**	**Reference**
GO-DPA	**Ni(II)**	180	293	6	1
GO/sawdust		138.31	298	6	2
GO		103	298	5.5	3
EDTA-GO		103	293	6.5	4
GO/PVA		62.3	303	5.7	5
G/MnO_2		46.6	298	5	6
GO/CNTs		40	298	5	7
GO-G		37	293	6	8
Fe_3O_4*-G*		22	293	6-7	9
Fe_3O_4*-GO-Chitosan*		12	293	5	10
GO_h/Tpy		**462**	**298**	**6**	**This work**
GO	**Zn(II)**	345	298	5	11
GO-PANI		297	303	6	12
GO		246	293	6	13
rGO		208	293	7	14
few layers GO		73	293	7	15
GO/CNTs		42	298	5	7
GO_h/Tpy		**421**	**298**	**6**	**This work**
$GO\text{-}NH_2$	**Co(II)**	116	298	6	16
GO/CD		72	303	6	17
Few layers GO		68,2	303	6	18
GO/CNTs		37	298	5	7
GO		21,3	298	5.5	19
M/GO		12.9	303	6	20
GO_h/Tpy		**336**	**298**	**6**	**This work**

Table S1. Comparative table for Ni(II), Zn(II) and Co(II) metal ions indicating the maximum adsorption capacity, temperature and pH of adsorption process on pristine GO and chemically modified GO materials.

Material	**C (w%)**	**N (w%)**	**O (w%)**
GO	55.89	0.27	39.63
GO$_h$	39.38	0.13	58.67
GO-Tpy	57.92	6.21	30.13
GO$_h$-Tpy	47.21	7.02	43.17

Table S2. Elemental atomic abundance of C, N, O obtained from the XPS survey spectra for GO, GO$_h$, GO-Tpy and GO$_h$-Tpy.

Material	**C (w%)**	**H (w%)**	**N (w%)**	**O (w%)**
GO	59.0	1.2	0	39.8
GO$_h$	41.3	2.1	0	56.6
GO-Tpy	59.3	1.0	5.9	33.8
GO$_h$-Tpy	45.9	1.5	7.4	45.2

Table S3. Elemental composition of GO, GO$_h$, GO-Tpy and GO$_h$-Tpy.

Material	**BET surface area (m^2 g^{-1})**	**Pore volume (cm^3 g^{-1})**	**Average pore size (nm)**
GO	16.2	0.09	6.4
GO$_h$	27.5	0.12	6.2
GO-Tpy	149.2	0.88	8.8
GO$_h$-Tpy	185.3	1.11	10.4

Table S4. Parameters obtained through the N_2 adsorption isotherm using the BET method.

Adsorbent	**Metal ions**	**Langmuir**			**Freundlich**		
		q_{max}	K_L [x10^{-2}]	R^2	n	K_F	R^2
GO	Ni(II)	285.4 ± 7	3.9 ± 0.4	0.995	3.3 ± 0.3	41 ± 7.8	0.949
	Zn(II)	259.6 ± 11.5	3.2 ± 0.4	0.998	2.5 ± 0.3	17.9 ± 3.1	0.926
	Co(II)	208 ± 9.2	1.2 ± 0.1	0.976	2.2 ± 0.3	13.5 ± 3.3	0.887
GO$_h$	Ni(II)	339.9 ± 13.2	9.7 ± 0.7	0.987	2.1 ± 0.2	18.2 ± 4.8	0.919
	Zn(II)	309.8 ± 12.3	9.8 ± 0.6	0.993	2.1 ± 0.2	14.9 ± 3.9	0.946

	Co(II)	249.2 ± 12.1	1.3 ± 0.1	0.983	2.1 ± 0.2	13.2 ± 3.1	0.896
GO-Tpy	Ni(II)	347 ± 12.2	2.5 ± 0.2	0.995	2.9 ± 0.3	49.5 ± 6.1	0.956
	Zn(II)	302.4 ± 10.5	1.7 ± 0.3	0.992	2.5 ± 0.3	33.3 ± 4.1	0.886
	Co(II)	255 ± 8.6	2.9 ± 0.4	0.993	3.2 ± 0.2	47.9 ± 4.8	0.971
GO_h-Tpy	**Ni(II)**	**462.7 ± 19**	**8.4 ± 0.5**	**0.995**	**1.9 ± 0.2**	**21.3 ± 2.5**	**0.938**
	Zn(II)	**421.5 ± 17.4**	**7.6 ± 0.5**	**0.996**	**1.8 ± 0.2**	**14.3 ± 2.6**	**0.959**
	Co(II)	**336.7 ± 12.5**	**8.9 ± 0.6**	**0.994**	**2.0 ± 0.2**	**15.4 ± 1.8**	**0.980**

Table S5. Parameters for Freundlich and Langmuir adsorption isotherms models of Ni(II), Zn(II) and Co(II) sorption on GO, GO_h, GO-TPy and GO_h-Tpy.

Parameters	**Ni(II)**	**Zn(II)**	**Co(II)**
Stability constant ($log\ k_1$)			
$Me^{2+} + OH^{-} \rightarrow Me(OH)^{+}$	4.97	4.4	4.3
$Me^{2+} + Ac \rightarrow Me(Ac)^{+}$	1.5	1.5	1.12
Ionic radius (pm)	69	74	74.5

Table S6. Parameters of first stability constant of the associated metal hydroxide and acetate and ionic radius for Ni(II), Zn(II) and Co(II) ions.

	Pseudo-first order kinetics			**Pseudo-second order kinetics**			$q_e(exp)$
	q_e	$k_1 x [10^{-2}]$	R^2	q_e	$k_2 x [10^{-5}]$	R^2	
Ni(II)	309 ± 11	1.44 ± 0.06	0.965	281 ± 9	3.9 ± 0.2	0.989	280 ± 10
Zn(II)	227 ± 9	2.01 ± 0.05	0.980	209 ± 8	9.3 ± 0.3	0.995	210 ± 8
Co(II)	152 ± 5	1.19 ± 0.09	0.982	186 ± 7	5.1 ± 0.2	0.996	180 ± 7

Table S7. Coordination kinetic rate constants and unit adsorption capacity of GO_h-Tpy towards metal ions.

	k_{p1} (mg/g $min^{1/2}$)	**k_{p2} (mg/g $min^{1/2}$)**	**C_1**	**C_2**	R_1^2	R_2^2
Ni(II)	18.42	2.46	35.15	170.8	0.996	0.901

Co(II)	11.05	2.44	20.22	94.40	0.998	0.968
Zn(II)	14.56	0.74	7.84	165.3	0.994	0.936

Table S8. Parameters of intra-particle diffusion model for Ni(II), Zn(II) and Co(II) adsorption onto GO$_h$-Tpy.

Metal ions	**T (K)**	**ΔG° (KJ mol^{-1})**	**ΔH° (KJ mol^{-1})**	**ΔS° (J mol^{-1}K^{-1})**	R^2
Ni(II)	298	-28.23	11.17	57.29	0.997
	308	-28.85			
	318	-39.37			
Co(II)	298	-28.06	10.23	59.83	0.999
	308	-28.67			
	318	-29.26			
Zn(II)	298	-27.84	8.02	66.48	0.99
	308	-28.49			
	318	-29.17			

Table S9. Thermodynamic parameters for adsorption of Ni(II), Zn(II), Co(II) onto GO$_h$-Tpy composite.

Experimental section

Preparation of GO and GO$_h$

Graphite (3.00 g, purchased from BAY CARBON Inc.) was stirred in 95% H_2SO_4 (75.0 mL). The required amount of $KMnO_4$ (4.50 and 9.00 g) was gradually added to the solution keeping the temperature <10 °C. The mixture was then stirred at 35 °C for 2 h. The resulting mixture was diluted by water (75.0 mL) under vigorous stirring. The suspension was further treated by adding 30% H_2O_2 solution (7.50 mL). The resulting graphite oxide suspension was purified by centrifugation with water. GOs samples were analyzed by C, H, N elemental analysis to evaluate the oxygen content. The result of elemental analysis is shown in Table S2.

Preparation and ^1H NMR characterization of Tpy

The preparation of the 4-(2,2':6',2"-terpyridin-4'-yloxy)butan-1-amine (Tpy) is based on previously described procedure[21] which was described below:
4-aminobutan-1-ol (4.0 g, 44.87 mmol) was added dropwise to a stirred suspension of powdered KOH (1.57 g, 27.98 mmol) in dry DMSO (20 mL) at 50 °C. After 20 min, 4’-chloro-2,2’:6’,2’’-terpyridine (3.0 g, 11.21 mmol) was added. The mixture was stirred at 50 °C for 3 h and then poured into deionized water (200 ml). The aqueous phase was extracted with DCM (5x 150 ml) and poured into ice to remove traces of DMSO still present in the organic phase. Biphasic mixture was separated, the organic phase was dried over $MgSO_4$, filtered and all the volatiles were evaporated to obtain Tpy as a light yellow solid (2.91 g, 81% yield), which was freeze dried until stable mass. The purity of obtained new Tpy molecules were controlled by H^1 NMR presented below.

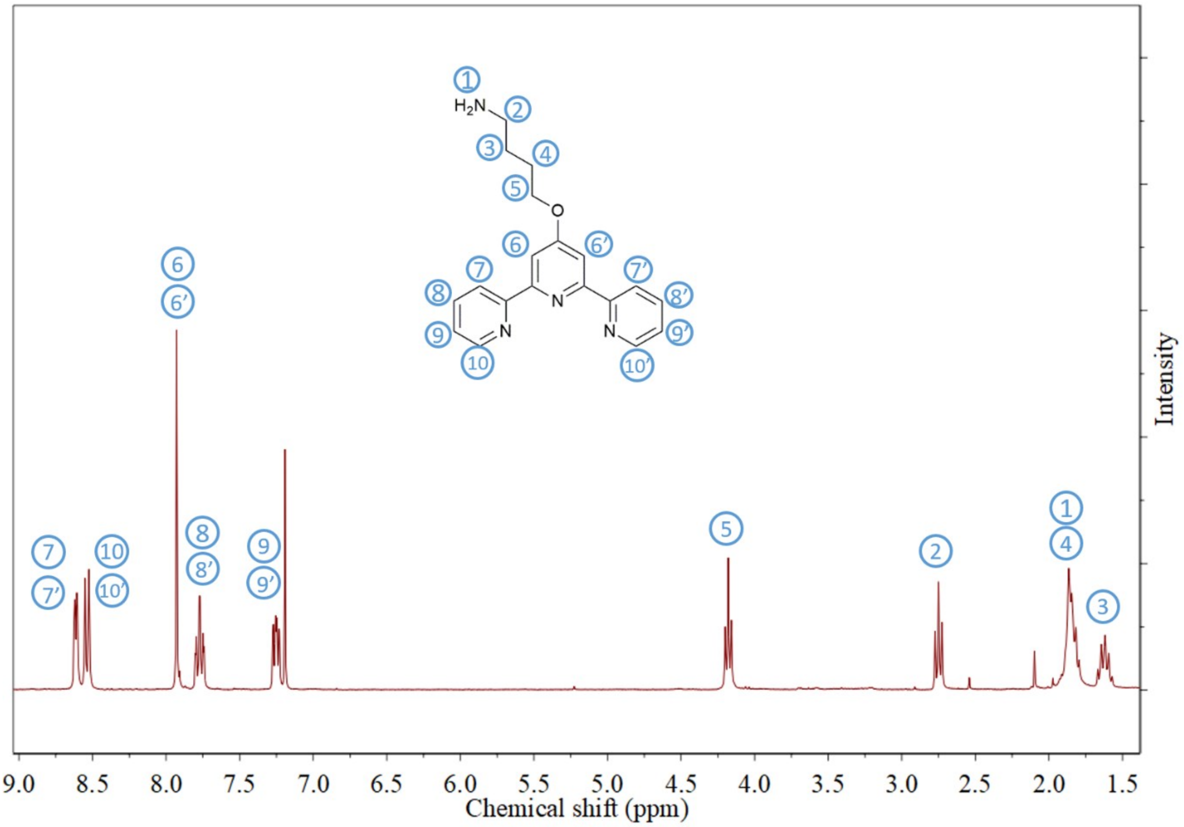

Fig. S1. ^{1}H NMR spectrum of Tpy.

^{1}H NMR (300 MHz, $CDCl_3$): δ 8.61 (2H, d, *J* = 4.0), δ 8.54 (2H, d, J = 8.0), δ 7.93 (2H, s), δ 7.77 (2H, ddd, J = 7.8, 1.8), δ 7.25 (2H, ddd, J = 7.4, 4.8, 1.1), δ 4.18 (2H, t, J = 6.3), δ 2.75 (2H, t, J = 7.1), δ 1.83 (4H, m), δ 1.62 (2H, m);

Estimation of the functionalization grade by XPS

The number of Tpy subunits in GO-Tpy as well as GO_h-Tpy hybrids per number of carbon atoms of GO was evaluated taking into account that any Tpy molecule contributes to the total number of carbon atoms “seen” by the XPS. For any nitrogen atom of the Tpy molecule there are 19 carbon atoms. Moreover from 4 nitrogen atoms in Tpy only one can react with oxygen atoms on GO. Therefore, the ratio of the number of carbon atoms of graphene oxide over the number of Tpy molecules ca be expressed as follows:

$$\frac{C_{GO-Tpy}}{Tpy_{molecules}} = \frac{C\%_{total} - 19 * (N\%_{total}/4)}{N\%_{total}/4} = \frac{57.92 - 19 * (\frac{6.21}{4})}{6.21/4} = 18.31$$

$$\frac{C_{GOh-Tpy}}{Tpy_{molecules}} = \frac{C\%_{total} - 19 * (N\%_{total}/4)}{N\%_{total}/4} = \frac{47.21 - 19 * (\frac{7.02}{4})}{7.02/4} = 7.90$$

We consider the functionalization degree is significantly higher in GO_h-Tpy preparation than GO-Tpy. Moreover, the ratio between the number of carbon atoms of graphene oxide over the number of N-containing terpyridine subunits is presented to provide a rough approximation on the structure of the hybrid materials.

Adsorption experiments

The batch adsorption experiments of the metal ions on GO-Tpy and GO_h-Tpy were investigated by mixing 10 mg of adsorbent with 50 ml of single-metal aqueous solutions with the desired pH and concentration. The pH of the solutions was adjusted using nitric acid or sodium hydroxide (0.1 M). For the sake of comparison, blank experiments in which neat compounds of GO with different oxidation degree (GO, GO_h) are used as adsorbents, are also carried out (see SI for more detail). The mixtures then were stirred at constant rate 200 rpm for 8 h at room temperature to attain equilibrium capacity. The adsorption analyses were performed by varying the following parameters: pH was varied from 2-10, temperature was varied in the range of 25-45 °C in the step of 10 C. Supernatant free solution was analysed using flame atomic absorption spectrometry (F-AAS). Especially, the amount of metal ions adsorbed on GO, GO_h GO-Tpy and GO_h-Tpy (q, mg g^{-1}) are calculated from the difference between the initial (C_0, mg L^{-1}) and the equilibrium concentration (C_e, mg L^{-1}) using the following equation (Eq.1):

$$q = \frac{(C_0 - C_e)V}{m_{ads}} \qquad Eq.1$$

where V is the volume of solution and m_{ads} is mass of used adsorbent. The metal ions removal efficiency was calculated using Eq.2:

$$Removal\,\% = \frac{(C_0 - C_e)V}{C_0} x\,100 \qquad Eq.2$$

The adsorption of metal ions on GO, GO_h, GO-Tpy and GO_h-Tpy was examined using two most commonly applied models for describing adsorption process on carbon-based adsorbents namely Langmuir and Freundlich. The Langmuir model (Eq.3) can be expressed as:

$$q_e = \frac{q_{max}K_LC_e}{1 + K_LC_e} \qquad Eq.3$$

where q_e is the amount of metal ions adsorbed on the adsorbent (mg g^{-1}), q_{max} is the maximum adsorption capacity (mg g^{-1}), K_L is the constant related to the free energy of adsorption (L mg^{-1}), C_e represents equilibrium concentration of metal ions in solution (mg L^{-1}). Otherwise, Freundlich isotherm model is represented by following equation (Eq.4):

$$q_e = K_FC_e^{1/n} \qquad Eq.4$$

where q_e and C_e are as defined above, K_F is the Freundlich constant related to the free energy of adsorption whereas n is the constant related to the adsorption intensity.

Kinetics and thermodynamics

In the present work, the kinetics of an adsorption process was examined on the most efficient material towards heavy metal ions *i.e.* GO_h-TPy hybrid using pseudo-first (Eq. 5) and pseudo-second (Eq. 6) order rate model as well as intraparticle diffusion model (Eq. 7).[76] The following linear equations can be expressed as:

$$\ln(q_e - q_t) = lnq_e - k_1t \quad Eq.5$$

$$\frac{t}{q_t} = \frac{1}{k_2q_e} + \frac{1}{q_e}t \qquad Eq.6$$

$$q_t = k_pt^{0.5} + C \qquad Eq.7$$

where q_e and q_t are the capacities of metal ions adsorbed at the equilibrium and time t (min), respectively, k_1 is pseudo-first order rate constant (min^{-1}), k_2 is the pseudo-second order rate constant (g min^{-1} mg^{-1}) and k_p is the intraparticle diffusion rate constant (mg g^{-1} $min^{-0.5}$). Symbol C (mg g^{-1}) in the equation is the constant which describes the boundary layer affects.

The thermodynamic parameters for heavy metal ions adsorption of GO_h-Tpy was obtained by using following equation:

$$\Delta G^0 = -RT\ln K_c \qquad Eq.8$$

Where ΔG^0 represents Gibbs energy change, R is the universal gas constant (8.3144 J mol^{-1} K^{-1}), T is absolute temperature in Kelvin and K_c is the equilibrium constant. The enthalpy (ΔH^0) and entropy (ΔS^0) changes can be calculated from the van't Hoff equation and more precisely from the slope and intercept, respectively, of a plot of $\ln K_c$ versus 1/T in according to equation:

$$\ln K_c = \frac{-\Delta H^0}{R} x \frac{1}{T} + \frac{\Delta S^0}{R} \qquad Eq.9$$

Experimental analysis

Raman analysis

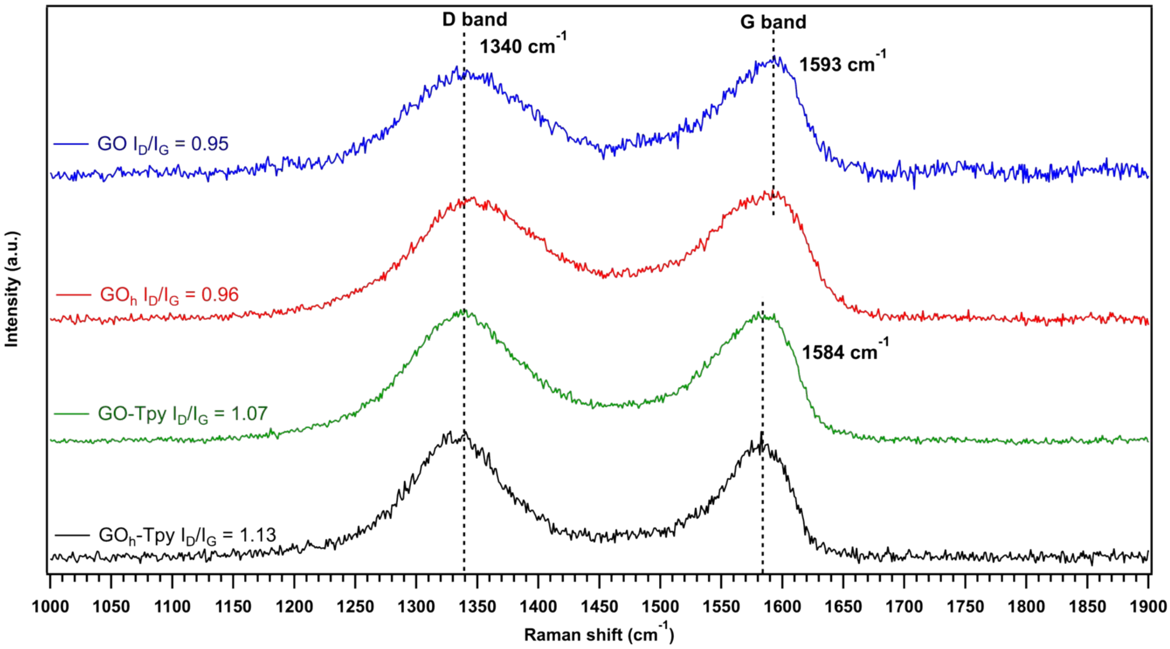

Fig. S2. Raman spectra recorded on GO, GO_h, GO-Tpy and GO_h-Tpy hybrids.

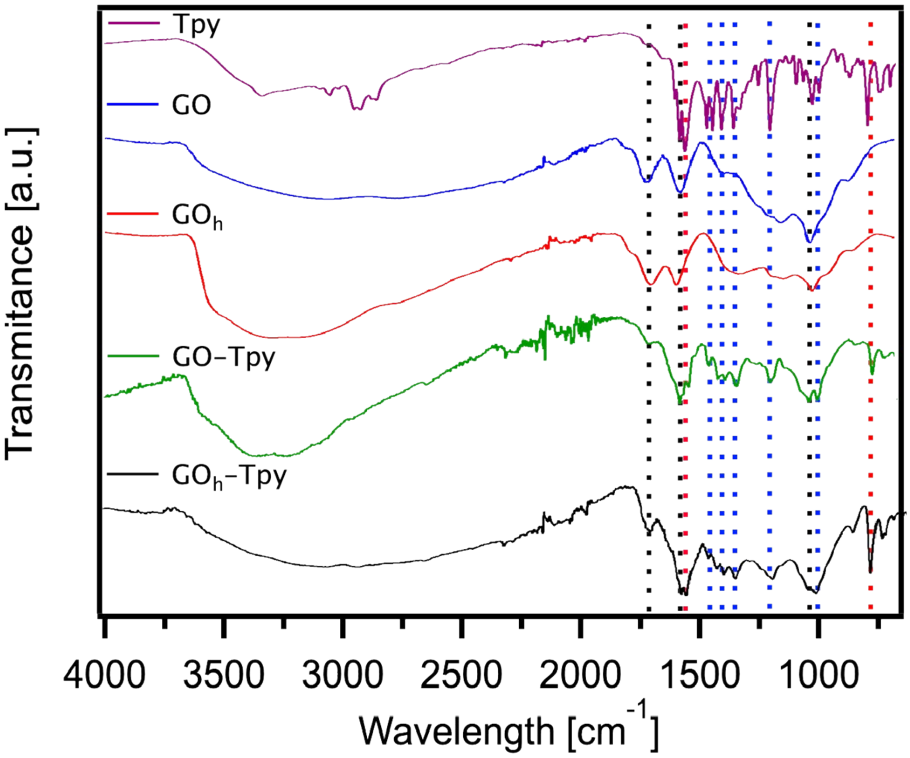

Fig. S3. Fourier transform infrared spectroscopy (FTIR) spectra of Tpy, GO, GO_h, GO-Tpy and GO_h-Tpy composites.

XPS analysis

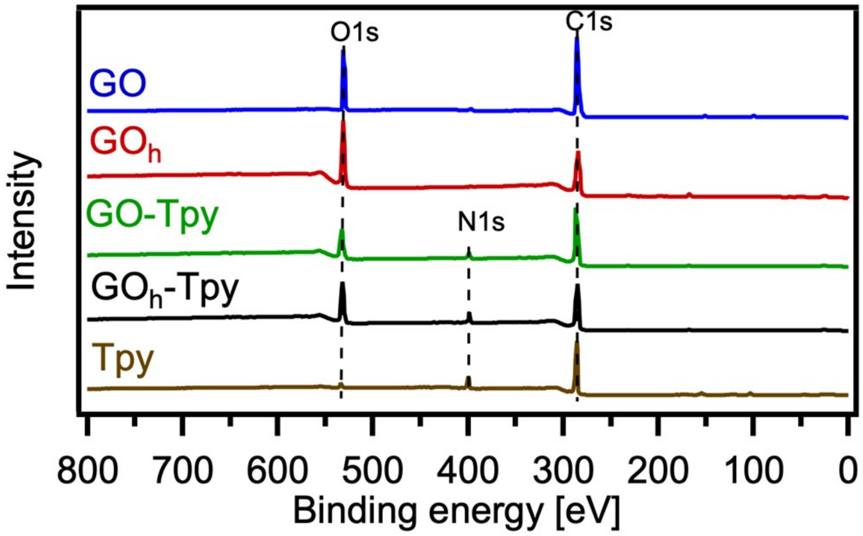

Fig. S4. XPS wide energy spectra of GO, GO_h, GO-Tpy, GO_h-Tpy and Tpy.

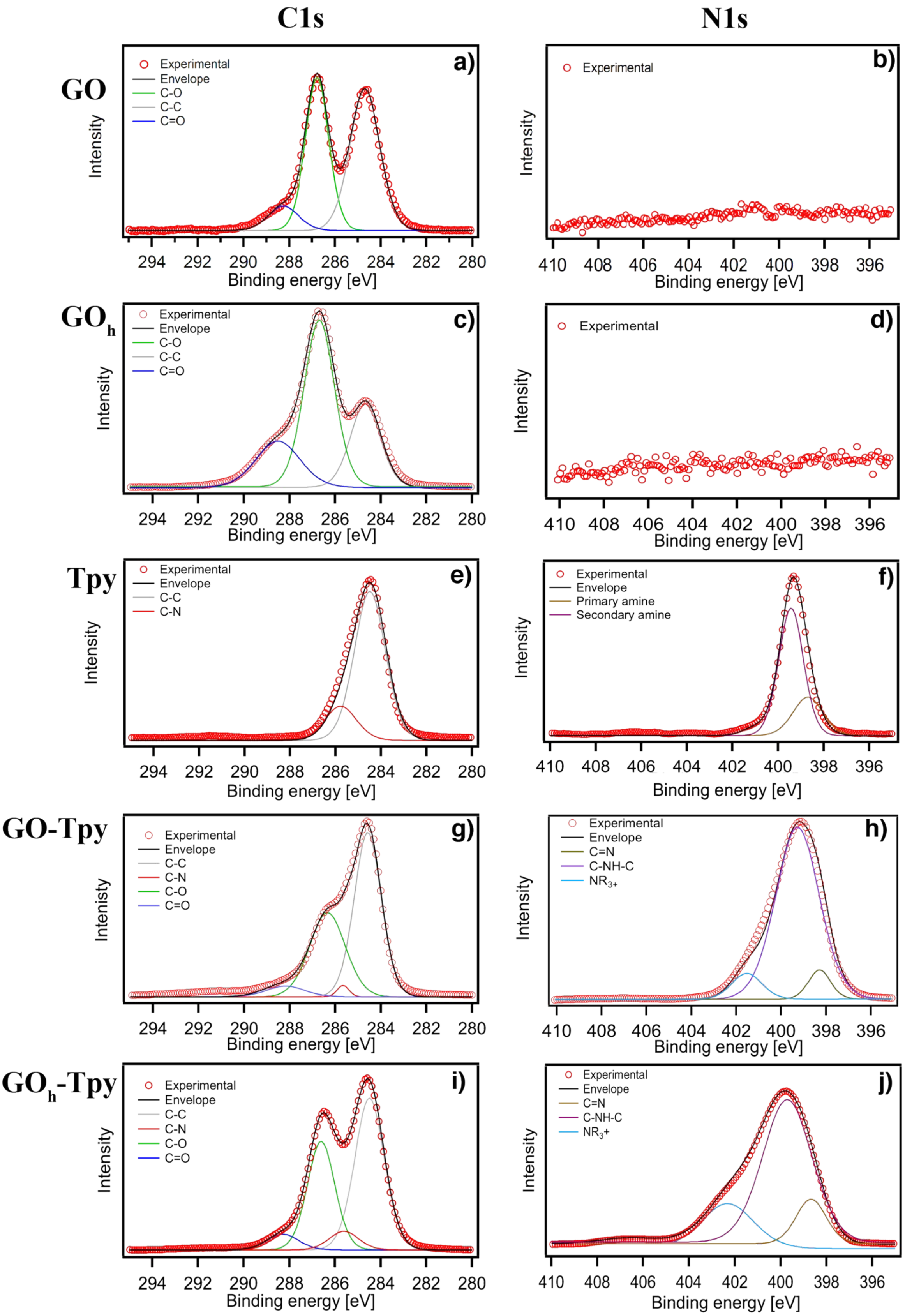

Fig. S5. XPS characterizations - High-resolution C1s, and N1s spectra of (a,b) GO, (c,d) GO$_h$, (e,f) Tpy, (g,h) GO-Tpy, (i,j) GO$_h$-Tpy. Experimental data are shown as red dots, and the individual deconvoluted components as coloured lines.

Average pore diameter of the GO_h*-Tpy composite*

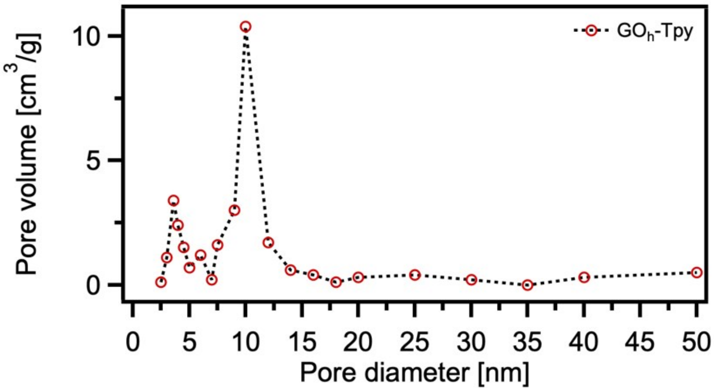

Fig. S6. Pore volume dV/dD plots for GO_h-Tpy.

TGA analysis

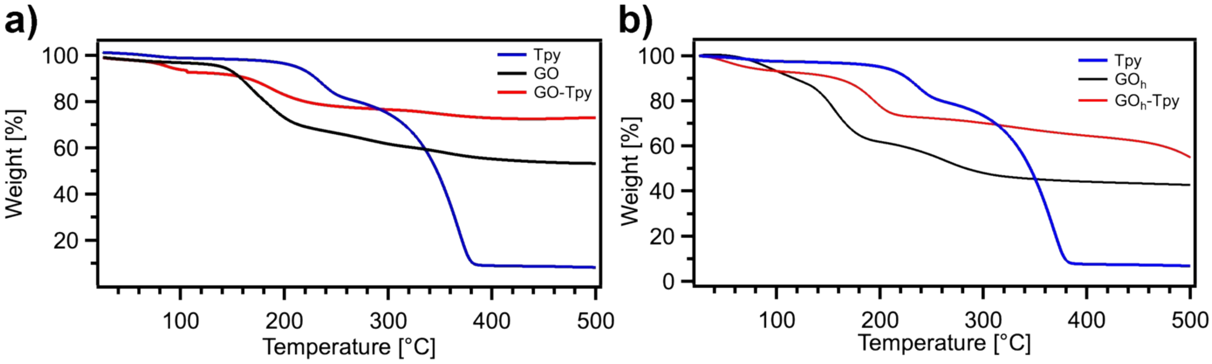

Fig. S7. Thermal decomposition of (a) Tpy, GO, GO-Tpy, and (b) Tpy, GO_h, GO_h-Tpy.

Adsorption capacity and zetapotential vs pH

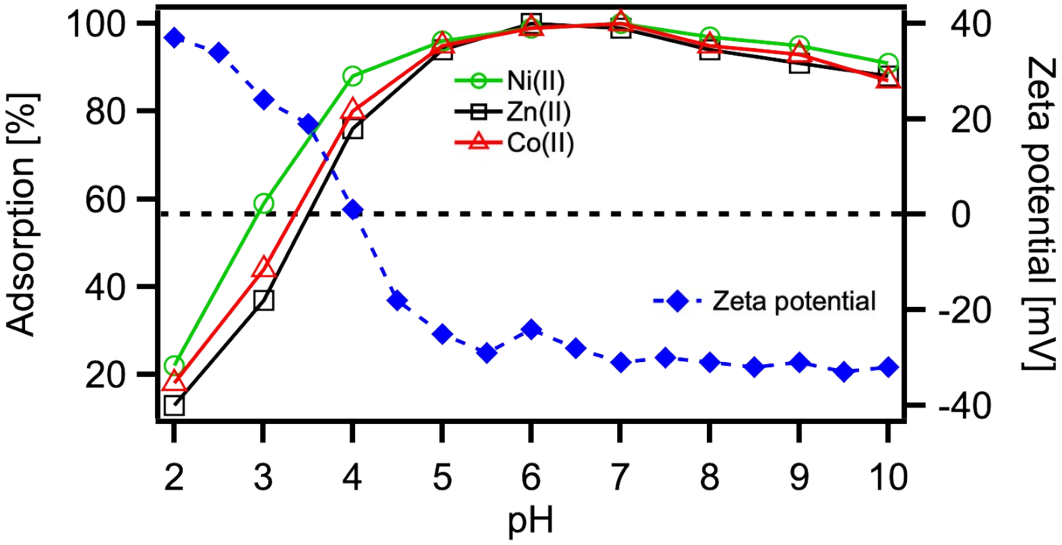

Fig. S8. Influence of pH on the adsorption process of Ni(II), Zn(II) and Co(II) on GO_h-Tpy composite with zeta potential of GO_h-Tpy (blue dotted line).

Metal species vs pH

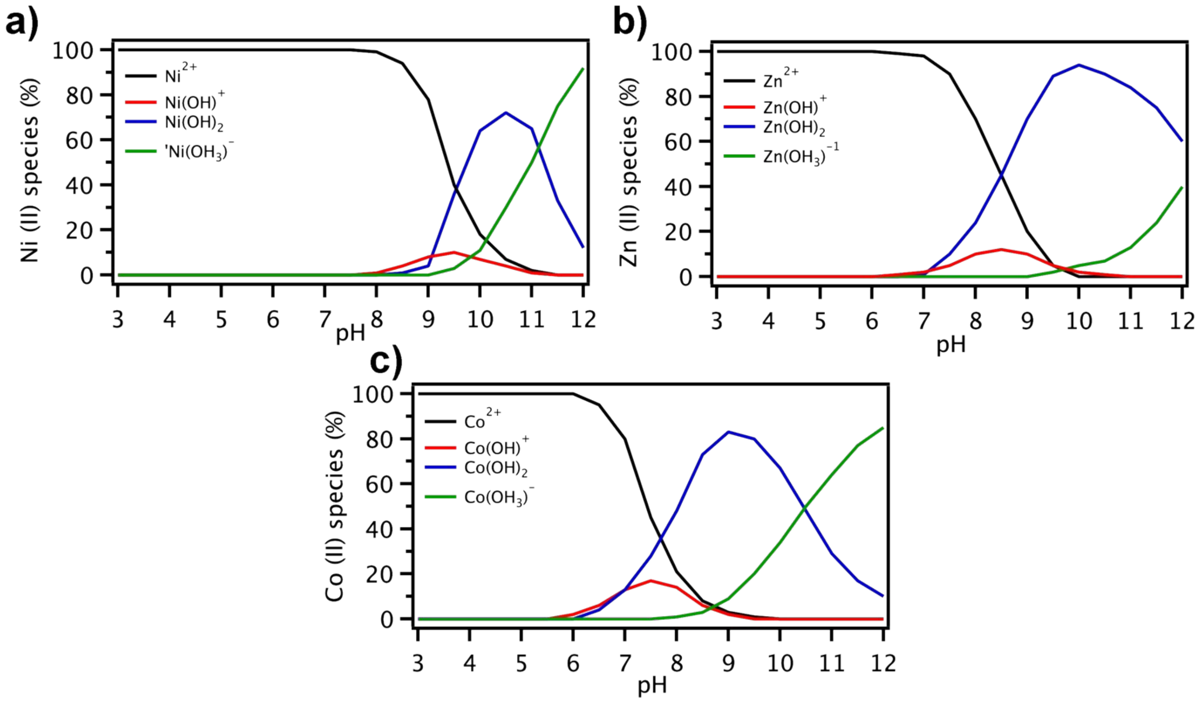

Fig. S9 Influence of pH of Ni(II) Zn(II) and Co(II) in aqueous solution. Graph was prepared in accordance to presented literature.[22-24]

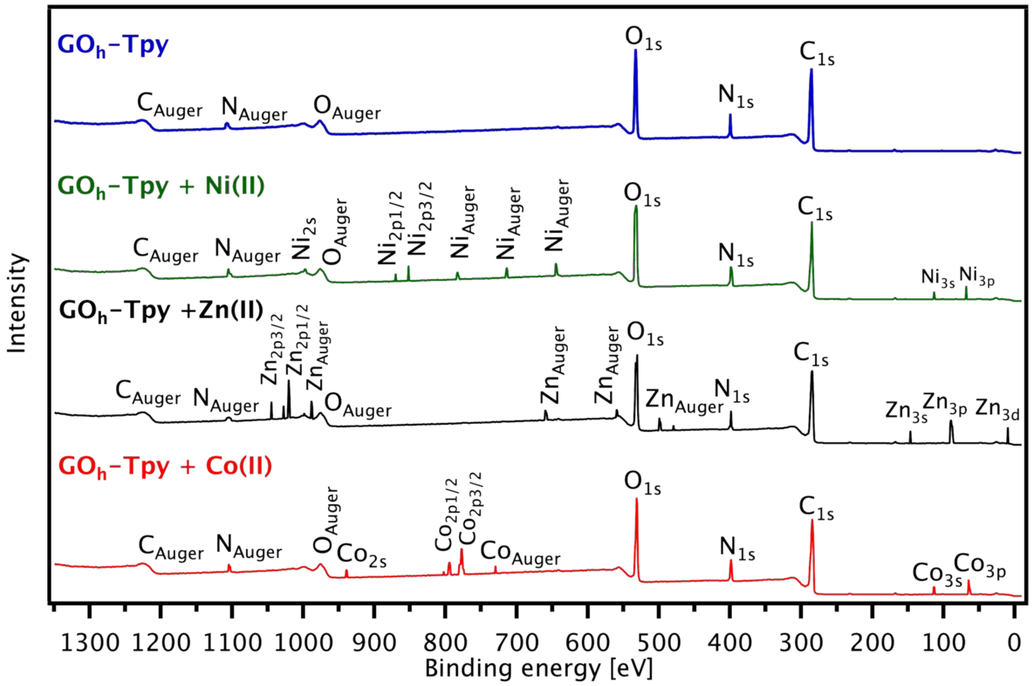

Fig. S10 The XPS spectra recorded before and after metal ions adsorption on GO$_h$-Tpy.

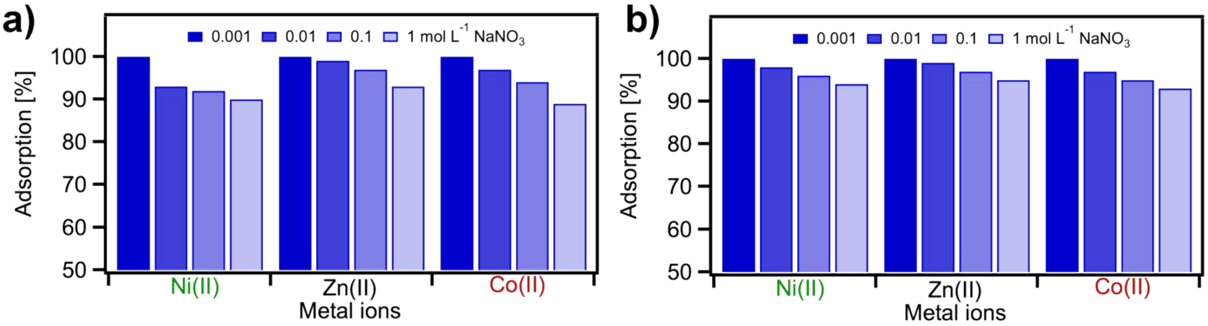

Fig. S11 Effect of ionic strength by NaNO$_3$ at different concentrations on (a) GO$_h$, and (b) GO$_h$-Tpy.

Thermodynamic study

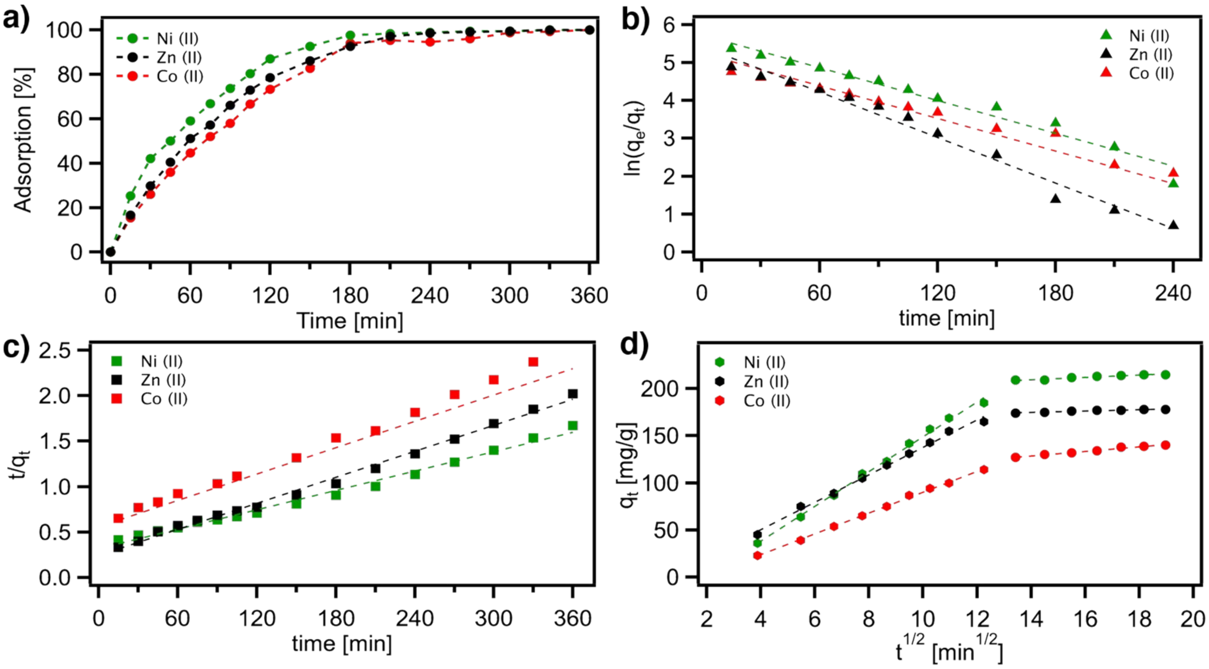

Fig. S12 Time dependent heavy metal ions sorption on GO$_h$-Tpy hybrid (a) (C_0 = 0.1 g L^{-1}, $C_{GO_h\text{-}Tpy}$ = 0.2 g L^{-1}, T = 25 °C, stirring speed = 200 rpm, t =8 h, pH = 6). The kinetic plots obtained with (b) pseudo-first, (c) pseudo- second order, and (d) intra-particle diffusion model reactions for GO$_h$-Tpy. In fig. (b), (c) and (d) intermittent lines represent linear function.

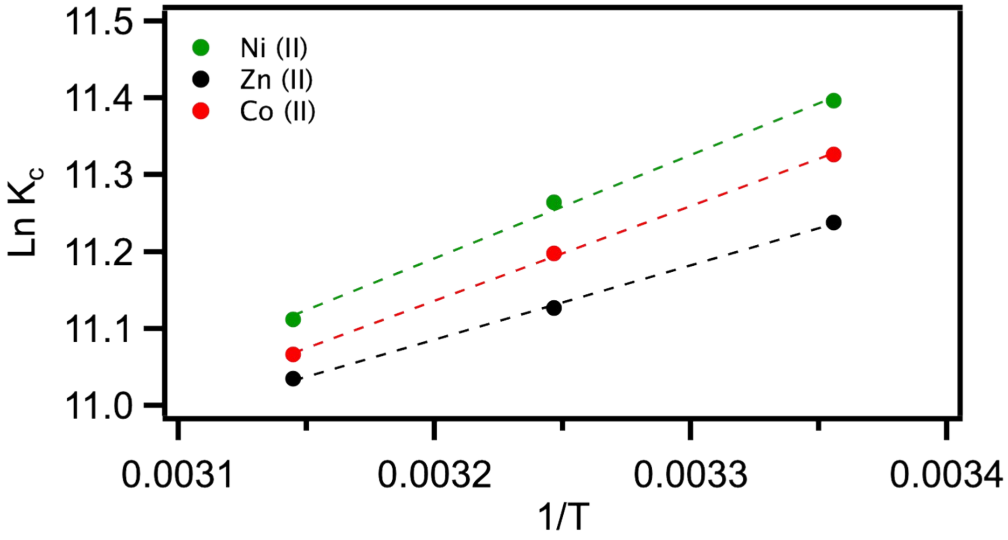

Figure S13. The linear curve of $\ln K_c$ vs 1/T for Ni(II), Zn(II), Co(II) adsorption to determine thermodynamic parameters for adsorption on GO_h-Tpy.

Reference

1. R. Zare-Dorabei, S. M. Ferdowsi, A. Barzin and A. Tadjarodi, *Ultrason. Sonochem.*, 2016, **32**, 265-276.
2. Y. Wu, H. Luo, H. Wang, L. Zhang, P. Liu and L. Feng, *J. Colloid Interface Sci.*, 2014, **436**, 90-98.
3. S. Yang, C. Chen, Y. Chen, J. Li, D. Wang, X. Wang and W. Hu, *ChemPlusChem*, 2015, **80**, 480-484.
4. C. Zhao, L. Ma, J. You, F. Qu and R. D. Priestley, *Desalin. Water Treat.* , 2016, **57**, 8942-8951.
5. P. Tan, J. Sun, Y. Hu, Z. Fang, Q. Bi, Y. Chen and J. Cheng, *J. Hazard. Mater.*, 2015, **297**, 251-260.
6. Y. Ren, N. Yan, Q. Wen, Z. Fan, T. Wei, M. Zhang and J. Ma, *Chem. Eng. J.*, 2011, **175**, 1-7.
7. M. Musielak, A. Gagor, B. Zawisza, E. Talik and R. Sitko, *ACS Appl. Mater. Interfaces*, 2019, **11**, 28582-28590.
8. F. Najafi, O. Moradi, M. Rajabi, M. Asif, I. Tyagi, S. Agarwal and V. K. Gupta, *J. Mol. Liq.*, 2015, **208**, 106-113.
9. X. Guo, B. Du, Q. Wei, J. Yang, L. Hu, L. Yan and W. Xu, *J. Hazard. Mater.*, 2014, **278**, 211-220.
10. L. T. Tran, H. V. Tran, T. D. Le, G. L. Bach and L. D. Tran, *Adv. Polym. Technol.*, 2019, **2019**.
11. R. Sitko, E. Turek, B. Zawisza, E. Malicka, E. Talik, J. Heimann, A. Gagor, B. Feist and R. Wrzalik, *Dalton Trans.*, 2013, **42**, 5682-5689.
12. M. Ramezanzadeh, M. Asghari, B. Ramezanzadeh and G. Bahlakeh, *Chem. Eng. J.*, 2018, **337**, 385-397.
13. H. Wang, X. Yuan, Y. Wu, H. Huang, G. Zeng, Y. Liu, X. Wang, N. Lin and Y. Qi, *Appl. Surf. Sci.*, 2013, **279**, 432-440.
14. M. Pan, G. Wu, C. Liu, X. Lin and X. Huang, *Nanomaterials*, 2018, **8**.
15. Q. Yang, G. Yang, W. Peng and S. Song, *Surf. Interface Anal.*, 2017, **49**, 398-404.
16. F. Fang, L. Kong, J. Huang, S. Wu, K. Zhang, X. Wang, B. Sun, Z. Jin, J. Wang, X.-J. Huang and J. Liu, *J. Hazard. Mater.*, 2014, **270**, 1-10.

17. W. Song, J. Hu, Y. Zhao, D. Shao and J. Li, *RSC Adv.*, 2013, **3**, 9514-9521.
18. G. Zhao, J. Li, X. Ren, C. Chen and X. Wang, *Environ. Sci. Technol.*, 2011, **45**, 10454-10462.
19. L. P. Lingamdinne, J. R. Koduru, H. Roh, Y.-L. Choi, Y.-Y. Chang and J.-K. Yang, *Hydrometallurgy*, 2016, **165**, 90-96.
20. M. Liu, C. Chen, J. Hu, X. Wu and X. Wang, *J. Phys. Chem. C*, 2011, **115**, 25234-25240.
21. Philip R. Andres, R. Lunkwitz, Gunther R. Pabst, K. Böhn, D. Wouters, S. Schmatloch and Ulrich S. Schubert, *European Journal of Organic Chemistry*, 2003, **2003**, 3769-3776.
22. K. Bellir, M. B. Lehocine and A.-H. Meniai, *Desalin. Water Treat.*, 2013, **51**, 5035-5048.
23. R. R. Sheha, S. I. Moussa, M. A. Attia, S. A. Sadeek and H. H. Someda, *Radiochimica Acta*, 2018, **107**, 67.
24. L. Fang, W. Li, H. Chen, F. Xiao, L. Huang, P. E. Holm, H. C. B. Hansen and D. Wang, *RSC Adv.*, 2015, **5**, 18866-18874.